Quantum dynamics of hard-core bosons in tilted bichromatic optical lattices

Xiaoming Cai, Shu Chen, and Yupeng Wang

Beijing National Laboratory for Condensed Matter Physics, Institute of Physics, Chinese Academy of Sciences, Beijing 100190, China

(Received 13 June 2011; published 6 September 2011)

We study the dynamics of strongly repulsive Bose gas in tilted or driven bichromatic optical lattices. Using the Bose-Fermi mapping and exact numerical method, we calculate the reduced single-particle density matrices, and study the dynamics of the density profile, the momentum distribution, and the condensate fraction. We show the oscillating and breathing mode of the dynamics, and the depletion of condensate for short-time dynamics. For long-time dynamics, we clearly show the reconstruction of system at integer multiples of Bloch-Zener time. We also show how to achieve clear Bloch oscillation and Landau-Zener tunneling for many-particle systems.

DOI: 10.1103/PhysRevA.84.033605 PACS number(s): 03.75.Lm, 05.30.Jp

I. INTRODUCTION

The dynamics of a particle in a period structure has been a fundamental subject, with the eigenenergies forming the famous Bloch bands [1] and the eigenstates being delocalized. If a weak external constant force is introduced, contrary to our intuition, the particle undergoes oscillatory motion rather than uniform motion due to acceleration by the force, which is known as the famous Bloch oscillation [1,2]. Under single-band tight-binding approximation, eigenenergies of the system form the Wannier-Stark ladder [3] with eigenstates localized. Bloch oscillation has been observed in semiconductor superlattices for electrons [4], optical lattices for cold atoms [2], and photonic crystals for light pluses [5,6]. For a stronger force, a directed motion is reintroduced by repeated Landau-Zener tunneling to higher Bloch bands [7–10]. For usual cosine-shaped potentials, band gaps decrease rapidly as the energy increases; this would lead to the decay of Bloch oscillation, which has been observed in Refs. [11–13].

In order to study the interplay between Bloch oscillation and Landau-Zener tunneling, one needs at least a two-band system with the lowest two bands well separated from the upper ones. Furthermore, the gap between the lowest two Bloch bands must be small for observing a clear signal of Landau-Zener tunneling. This can be achieved by bichromatic optical lattices [14], where parameters of the system are adjustable and controllable. Bichromatic lattices have been implemented by superimposing two incoherent optical lattices, with the wavelength of one lattice two times the other [15,16], or by virtual two-photon and four-photon processes [17–21]. Under two-band tight-binding approximation, eigenenergies form two Wannier-Stark ladders with energy spacing doubled and an offset between them [22,23]. The corresponding eigenstates are still localized. The dynamics of a particle is governed by two timescales, i.e., the Bloch period and the period of Zener oscillation. If the two periods are commensurate, the system reconstructs at integer multiples of Bloch-Zener time.

So far, most works concentrate on the dynamics of the single-particle system. The generalization of these results to interacting many-particle systems remains an open question. The possibility of investigating Bloch oscillation and Landau-Zener tunneling of interacting Bose-Einstein condensate (BEC) experimentally has attracted much interest. Most theoretical studies are based on the mean-field approximation [24–27] and Gross-Pitaevskii (GP) equations [28]. Results for the dynamics of strongly interacting many-particle systems are rarely known. In this paper, we study the dynamics of interacting bosons in bichromatic optical lattices under constant drag force in the limiting case with infinitely repulsive interaction, which permits us to solve the problem exactly. The one-dimensional (1D) Bose gas with infinitely repulsive interaction is known as the hard-core boson (HCB) or Tonks-Girardeau (TG) gas [29], which can be exactly solved via the Bose-Fermi mapping [29], and has attracted intensive theoretical attention [30–32]. Experimental access to the required parameter regime has made the TG gas a physical reality [33,34]. Following the exact numerical approach proposed by Rigol and Muramatsu [35,36], we calculate the dynamics of density profile, momentum distribution, and condensate fraction for hard-core bosons in the tilted bichromatic optical lattice, and show Bloch oscillation, Landau-Zener tunneling, and reconstruction of the system at integer multiples of Bloch-Zener time.

The paper is organized as follows. In Sec. II, we present the model and the exact approach used in this paper. We also recover the dynamics of the single-particle system in this section. In Sec. III, we study the short-time and long-time dynamics for hard-core bosons in bichromatic optical lattice with a constant drag force. We also show how to achieve clear Bloch oscillation and Landau-Zener tunneling for the many-particle system. Finally, a summary is presented in Sec. IV.

II. MODEL AND METHOD

In this section we describe the exact approach we used to study 1D hard-core bosons in tilted or driven bichromatic optical lattices. Under the tight-binding approximation, the system can be described by the following Hamiltonian:

$$H = -J\sum_i (b_i^\dagger b_{i+1} + \text{H.c.}) + \delta\sum_i (-1)^i n_i^b + F\sum_i i n_i^b + \sum_i V_i n_i^b. \quad (1)$$

Here we only consider the nearest-neighbor hopping and neglect the off-diagonal terms of position operator $\hat{x}$ in the Wannier basis. The operator $b_i^\dagger$ (b_i) is the creation (annihilation) operator of the boson which fulfills the hard-core constraints [35], i.e., the on-site anticommutation ($\{b_i, b_i^\dagger\} =$

1) and $[b_i, b_j^\dagger] = 0$ for $i \neq j$; n_i^b is the bosonic particle number operator; J is the hopping amplitude being set to be unit of energy ($J = 1$); $V_i = V_H(i - i_0)^2$ is the harmonic potential for preparing the initial state of the system, with V_H the strength and i_0 the position of the trap center; δ is the energy shift of the alternate site; and F is the strength of driven force. For convenience, the lattice spacing is set to be the unit of measure.

In order to study the dynamics of the hard-core bosons in a driven optical lattice, we first load the hard-core bosons into a bichromatic optical lattice with an additional harmonic trap. Then we switch off the harmonic trap and turn on the driven force. We shall study the evolution of the initially prepared system and the dynamics of the system under the driven force. First, the initial state is the ground state of the Hamiltonian:

$$H_{\text{init}} = -J \sum_i (b_i^\dagger b_{i+1} + \text{H.c.}) + \delta \sum_i (-1)^i n_i^b + \sum_i V_i n_i^b, \tag{2}$$

with particle number N. In order to get the initial state, it is convenient to use the Jordan-Wigner transformation [37] (JWT),

$$b_j^\dagger = f_j^\dagger \prod_{\beta=1}^{j-1} e^{-i\pi f_\beta^\dagger f_\beta}, \quad b_j = \prod_{\beta=1}^{j-1} e^{+i\pi f_\beta^\dagger f_\beta} f_j, \tag{3}$$

to map the Hamiltonian of hard-core bosons into the Hamiltonian of noninteracting spinless fermions H_{init}^F, which is in the same form as H_{init}, but with all the boson operators, e.g., $b_i^\dagger$, b_i, and n_i^b, being replaced by the corresponding fermion operators, e.g., $f_i^\dagger$, f_i, and n_i^f. The ground-state wave function of the system with N spinless free fermions, which is a product of lowest N eigenfunctions, can be obtained by diagonalizing H_{init}^F and can be represented as

$$|\Psi_F^G\rangle = \prod_{n=1}^{N} \sum_{i=1}^{L} P_{in} f_i^\dagger |0\rangle, \tag{4}$$

where L is the number of lattice sites, N is the number of fermions (same as bosons), and coefficients P_{in} are the amplitude of the nth single-particle eigenfunction at the ith site which can form an $L \times N$ matrix P [38].

After releasing from the trap, the system is described by the Hamiltonian:

$$H_e = -J \sum_i (b_i^\dagger b_{i+1} + \text{H.c.}) + \delta \sum_i (-1)^i n_i^b + F \sum_i i n_i^b. \tag{5}$$

Similar to the above method, from the corresponding free-fermion Hamiltonian H_e^F, we can get all single-particle states and corresponding energies, and use P' to represent all the single-particle states and ε_i to represent the energies. The nonequilibrium quantum dynamical properties of the system can be calculated through the equal time one-particle Green function which is defined as

$$G_{ij}(t) = \langle \Psi_{\text{HCB}}(t) | b_i b_j^\dagger | \Psi_{\text{HCB}}(t) \rangle, \tag{6}$$

where $|\Psi_{\text{HCB}}(t)\rangle$ is the wave function of hard-core bosons at time t after releasing from the harmonic trap. After some derivations (see Appendix A), one can get

$$G_{ij}(t) = \det[(P^A)^\dagger P^B], \tag{7}$$

where P^A and P^B are obtained from P, P', and ε_i. It follows that the reduced single-particle density matrix can be determined by the expression

$$\rho_{ij}(t) = \langle b_i^\dagger b_j \rangle_t = G_{ji}(t) + \delta_{ij}[1 - 2G_{ii}(t)]. \tag{8}$$

The momentum distribution is defined by the Fourier transform with respect to $i - j$ of the reduced single-particle density matrix with the form

$$n(k) = \frac{1}{L} \sum_{i,j=1}^{L} e^{-ik(i-j)} \rho_{ij}, \tag{9}$$

where k denotes momentum. The natural orbitals ϕ_i^η are defined as eigenfunctions of the reduced single-particle density matrix [39],

$$\sum_{j=1}^{L} \rho_{ij} \phi_j^\eta = \lambda_\eta \phi_i^\eta. \tag{10}$$

The natural orbitals can be understood as being effective single-particle states with occupations λ_η. For noninteracting bosons, all particles occupy the lowest natural orbital and bosons are in the BEC phase at zero temperature, whereas only the quasicondensation exists for 1D hard-core bosons [35].

For hard-core bosons we know that the state for the corresponding Fermi Hamiltonian is a product of time-dependent single-particle states, and each single-particle state evolves itself (see Eq. [(A4)] in Appendix A). We recover the single-particle properties of the Hamiltonian H_e in Appendix B, which have been studied by Breid *et al.* [22]. From Appendix B, we know that a single-particle wave function will be reconstructed at integer multiples of Bloch-Zener time (T_{BZ}) if T_1 and T_2 are commensurate. Here T_1 is the Bloch period decided by the spacing of the Wannier-Stark ladders, and T_2 is the period of Zener oscillation decided by the offset between Wannier-Stark ladders. Since each single-particle state can be reconstructed at a period of time, and the period is independent of the single-particle state and decided by parameters of Hamiltonian, the state for many-body hard-core bosons composed of a product of single-particle states will also be reconstructed at integer multiples of Bloch-Zener time.

III. QUANTUM DYNAMICS OF HARD-CORE BOSONS

In order to observe reconstruction of the system, two periods T_1 and T_2 must be commensurate, which are decided by F and E_0, where E_0 is a function of F and δ. In Fig. 1(a), we show numerical results of E_0 versus δ for a particular F. For different F, structure of the picture is similar. In order to generate a particular Bloch-Zener time (T_{BZ}), δ must be one of the discrete numbers. For example, if we want $T_{\text{BZ}} = T_B$ for the system with $F = 0.05$, we have to let $E_0 = 0$ and then $\delta = 0.1684, 0.3614, \ldots$.

For comparison, we first recover the dynamics of a single-particle system. We choose $E_0 = 0$ and let the system

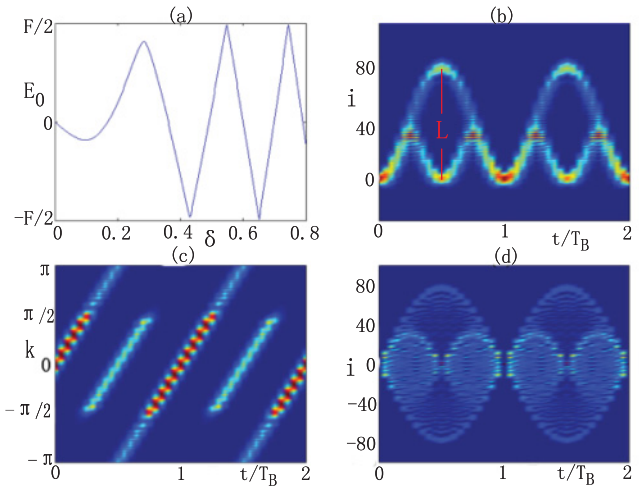

FIG. 1. (Color online) (a) E_0 vs δ for the system with $F = 0.05$. The dynamics of the density profile (b) and momentum distribution (c) for the single-particle system with $\delta = 0.1684$, $F = 0.05$, and $V_H = 0.001$. (d) The breathing mode dynamics of the density profile for the single-particle system with $\delta = 0.1684$, $F = 0.05$, and $V_H = 20$.

reconstruct at integer multiples of Bloch time (T_B). From now on, we take Bloch time $T_B = 2T_1$ as the reference timescale. In Fig. 1(b), we show the dynamical evolution of the density profile for a single-particle system, from which one can see the reconstruction of the density profile at integer multiples of Bloch time. The edge of the Brillouin zone is reached at $t = T_B/4$, and part of the particle moves into the upper excited Bloch band located in the upper half of the figure. The particle in the upper excited band returns to the lower Bloch band at $t = 3T_B/4$. For a quantitative analysis of the Landau-Zener tunneling rate, one can characterize it by the number of particles in the upper half of the picture at time $t = T_B/2$. Numerical results show that the Landau-Zener tunnelling probability [28]

$$P_{\mathrm{LZ}} \approx \exp\left(-\frac{\pi\delta^2}{2F}\right). \tag{11}$$

So in order to see a clear signal of Landau-Zener tunneling, we have to choose small δ for a given strength of force F. Furthermore, the available interval for motion of a particle in lattice [40]

$$L \approx 4/F. \tag{12}$$

In Fig. 1(c), we also show the dynamical evolution of momentum distribution of the single-particle system. Particles with momentum in the interval $(-\pi/2,\pi/2)$ are in the lower Bloch band, and outside the region particles are in the upper excited Bloch band. From this picture we can see the clear signals for Bloch oscillation and Landau-Zener tunneling. Furthermore the momentum is linear with time with slope given by F. Next we consider a localized initial state which has a wide momentum distribution and can be implemented by setting a strong harmonic trap potential, for example, $V_H = 20$ here. From Fig. 1(d), one can find a breathing behavior of the density profile. The reconstruction still happens at integer multiples of T_B. But one can observe that the enveloping structure with period of T_B is overlayed by a breathing mode of smaller amplitude, whereas part of the particle remains in the lower Bloch band all the time with a period of $T_B/2$.

Now we consider the case of many-body hard-core bosons and study the short-time dynamics first. Systems with various particle numbers will be considered by keeping the other parameters fixed. For comparison, we show the dynamics of a single-particle system in the first column of Fig. 2. After release from the trap, the particle speeds up under the drag force F, and it reaches the edge of the Brillouin zone at time $T_B/4$. Part of the particle moves into the upper excited Bloch band through Landau-Zener tunneling, while the other part of the particle remains in the lower Bloch band with changing of the sign of momentum by Bragg scattering. Because of Landau-Zener tunneling, the particle turns into two parts separated in real space, with particles in the upper half of the density distribution being in the upper excited Bloch band. In the momentum distribution, the particles outside the first Brillouin zone of $(-\pi/2,\pi/2)$ are in the upper excited Bloch band. The changing of the sign of momentum occurs at time $T_B/4$ by Bragg scattering for particles in the lower Bloch band. In the third row of Fig. 2, we show the evolution of condensate fraction which is defined as λ_0/N with λ_0 being the occupation of the lowest effective single-particle state. For the single-particle system, the particle is always in the lowest effective single-particle state, and the condensate fraction is one all the time. For the 1D many-body systems of hard-core bosons, there is only quasicondensation with $\lambda_0 \propto \sqrt{N}$ [29,35]. In the fourth row of Fig. 2, we show the reduced single-particle density matrix at time $T_B/2$. Here we consider the modulus because of the elements of the density matrix being complex numbers after turning off the trap. The upper right spot in the picture is caused by particles in the upper excited Bloch band and the lower left spot for the lower Bloch band. For single-particle dynamics, however, particles in the upper excited Bloch band and the lower Bloch band are separated in real space, there is phase coherence between them, and the off-diagonal parts of the reduced single-particle density matrix are very strong.

In the second through fifth columns, we show the dynamics for the hard-core bosons with $N = 2,5,30$, and 150, respectively. As the particle number increases, the adding particle has to occupy a higher single-particle state because one state can only be occupied by a hard-core boson. And the size (S) of system becomes larger and larger, while the available interval L of the system decided by force F remains unchanged. Also, the width of the momentum distribution becomes wider for the larger system. As the momentum distribution becomes wider, it takes a shorter time for particles at the edge of the momentum distribution to reach the edge of the Brillouin zone, and thus Landau-Zener tunneling happens early, which leads to the condensate fraction decreasing early. The condensate fraction decreases ($\propto 1/\sqrt{N}$) as the particle number increases. As time increases but is smaller than $T_B/4$, the condensate fraction basically does not change. A slight increase of the condensate fraction in short time is caused by the expansion after turning off the trap [38]. At time $t = T_B/4$, Landau-Zener tunneling happens, and the condensate fraction decreases quickly. After this an overdamped area appears, and then

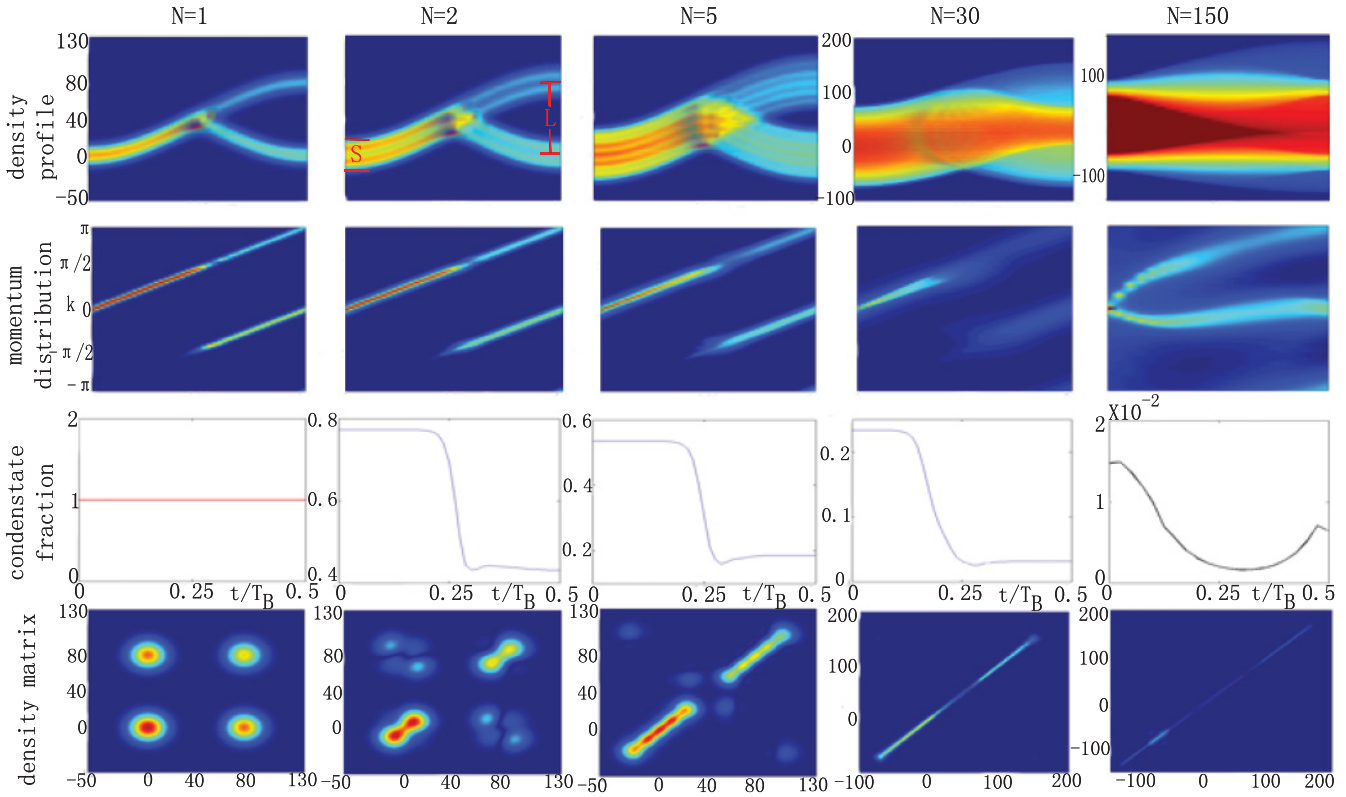

FIG. 2. (Color online) The short-time dynamical evolution of density profile (first row), momentum distribution (second row), condensate fraction (third row), and modules of the reduced single-particle density matrix (fourth row) at time $t = T_B/2$ for systems of different particle number with $F = 0.05$, $\delta = 0.1684$, $E_0 = 0$, and $V_H = 10^{-4}$ ($V_H = 8 \times 10^{-4}$ for the fifth column).

the condensate fraction remains basically unchanged. For the reduced single-particle density matrix at time $T_B/2$, lengths for the two parts of the diagonal terms become larger as the size (S) of the system increases. The off-diagonal parts of the matrix become weaker as particles are added in. Also, the phase coherence between particles in the upper excited Bloch band and the lower Bloch band decreases. As shown in the figure, the particles between the upper band and the lower band lost their phase coherence when $N = 30$. Furthermore, the particles in the upper excited Bloch band and the lower Bloch band developed phase coherence inside each part; the reduced single-particle density matrix has exponential law decay in each part as the distance increases.

We note that the density profile no longer splits into two obviously separated parts after time $T_B/4$ for system with $N = 30$ as shown in the fourth column, where the particles in the upper excited Bloch band and the lower Bloch band are overlapped in real space. To achieve this situation, one has to adjust the parameters of the system and let the size of the system be larger than the available interval ($S > L$). One also has to avoid the initial state staying in a localized state because a localized initial state will cause the breathing mode dynamics. Although the two parts are overlapped in real space, they are separated in the momentum distribution. The width of the momentum distribution becomes larger as the particle number increases. The dynamical evolution of condensate fraction still has a similar structure, except that the quick decrease happens earlier. As two parts of particles are overlapped in real space, the diagonal terms of the density matrix are also overlapped. For sites outside the overlapped area in the upper excited Bloch band or the lower one, the density matrix still has an exponential law decay as distance increases. For the overlapped area the density matrix is irregular, but as the distance increases, it goes to zero quickly. In the fifth column, we show the dynamics of the system with $N = 150$. As the particle number increases, the localization of the initial state becomes stronger [35] and we see the breathing mode of the dynamics of the density distribution. Lots of particles are localized in the center, and particles in two parts are overlapped. The dynamics of the momentum distribution is also changed. The momentum distribution does not increase linearly as time increases, and momentum distributions for particles in the upper excited Bloch band and lower Bloch band are overlapped. For the localized initial state, the momentum distribution is almost flat. Right after turning off the trap, there are particles moving into the upper excited Bloch band through Landau-Zener tunneling, and the condensate fraction decreases immediately. Meanwhile, for a localized initial state, the expansion is also important after turning off the trap, and there is a large overdamped area in the breathing mode dynamics of the condensate fraction. The reduced single-particle density matrix still has exponential law decay for particles in localized states.

Next, we consider the long-time dynamics of hard-core bosons. In Fig. 3(a), we show the dynamical evolution of density distribution for a five-particle system with Bloch-Zener

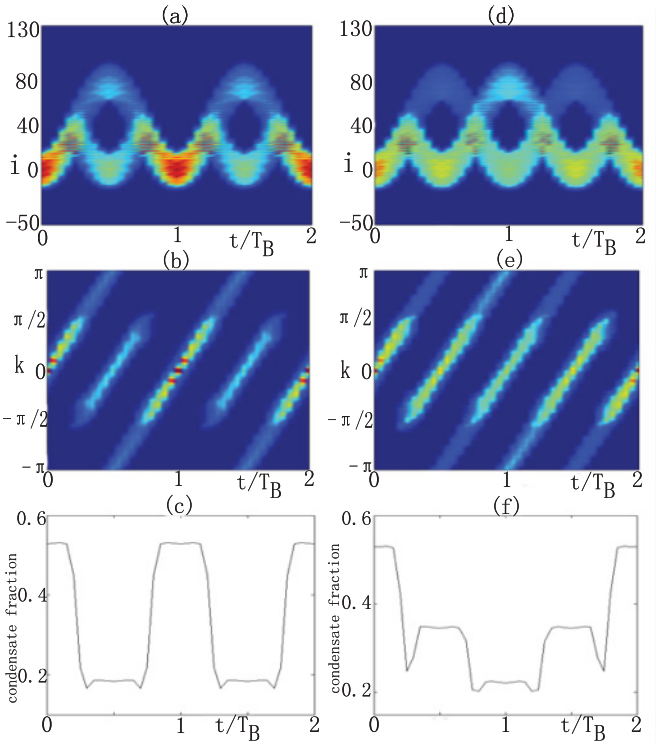

FIG. 3. (Color online) The dynamical evolution of density profile (a,d), momentum distribution (b,e), and condensate fraction (c,f) for the five-particle system with $F = 0.05$, $V_H = 10^{-3}$, and $\delta = 0.1684$ (a,b,c), $\delta = 0.238$ (d,e,f).

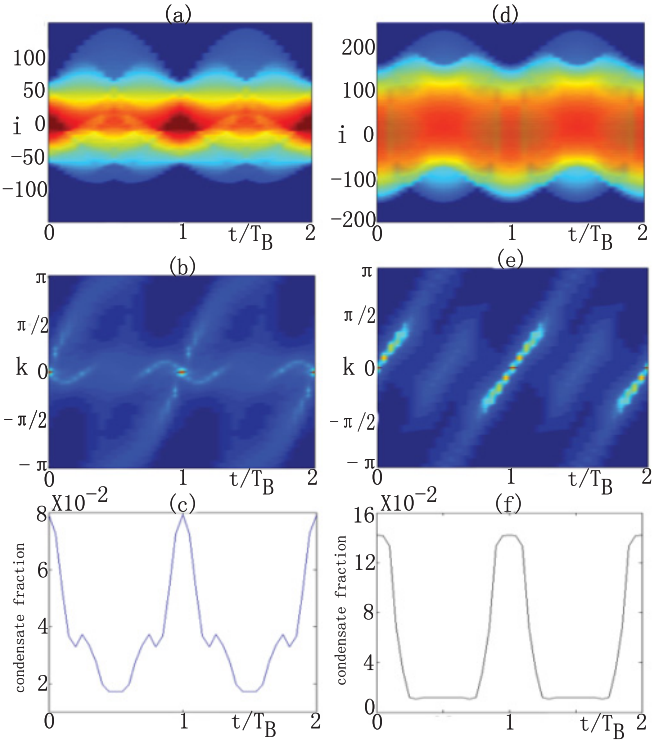

FIG. 4. (Color online) The dynamical evolution of density profile (a,d), momentum distribution (b,e), and condensate fraction (c,f) for the 80-particle system with $F = 0.05$, $\delta = 0.1684$, and $V_H = 10^{-3}$ (a,b,c), $V_H = 4 \times 10^{-5}$ (d,e,f).

time $T_{\mathrm{BZ}} = T_B$, where $E_0 = 0$. After releasing from the harmonic trap, particles move along with the direction of the force F. Around time $t = T_B/4$, particles reach the edge of the Brillouin zone, and part of the particles move into the upper excited Bloch band through Landau-Zener tunneling and keep moving along with force F. The other part of the particles remain in the lower Bloch band, but the momentum of the particles changes the sign due to Bragg scattering and thus the particles move against the force F. Around time $t = 3T_B/4$, particles reach the edge of Brillouin zone again, and all particles move into the lower Bloch band. At time $t = T_B$, the system reconstructs into the initial state. As time goes on, more periods occur. The dynamical evolution of the momentum distribution for the same system is shown in Fig. 3(b). After turning off the trap, particles accelerate under force F, and the momentum increases linearly with time. Around time $t = T_B/4$, particles reach the edge of the Brillouin zone ($k = \pi/2$). Part of the particles, which move into the upper Bloch band through Landau-Zener tunneling, remain in the same belt and their momentum increases linearly with time. The other part of the particles stay in the lower Bloch band and change the sign of their momentum by Bragg scattering. Two parts of particles are recombined around time $t = 3T_B/4$, and the momentum distribution returns to the initial distribution at $t = T_B$. In Fig. 3(c), we show the dynamical evolution of the condensate fraction. Around time $t = T_B/4$, the condensate fraction has a quick decrease due to Landau-Zener tunneling. After this there is an overdamped area. Around time $t = 3T_B/4$, two parts of the particles recombine, and the condensate fraction increases quickly. The system returns to its initial state at time $T = T_{\mathrm{BZ}}$. Furthermore, the condensate fraction is symmetrical with center at $T = T_{\mathrm{BZ}}/2$. In Fig. 3, we also show the dynamics of a system with $T_{\mathrm{BZ}} = 2T_B$ where $E_0 = F/4$, which has similar properties to the previous one. From Fig. 3(d), one can obviously observe the reconstruction of the system after Bloch-Zener time T_{BZ}, Bloch oscillation, and Landau-Zener tunneling.

In Fig. 4, we show the dynamical evolution of a system with 80 hard-core bosons. As particles add in, the particles in the initial state get more localized, and the dynamical evolution of the system is dominated by the breathing mode instead of the oscillating mode. In Fig. 4(a), we show the dynamical evolution of the density profile for a system with $F = 0.05$, $\delta = 0.1684$, and $V_H = 10^{-3}$. This picture is not in prefect breathing mode because of the initial state being not localized enough. First of all, the reconstruction of density profile happens again after integer multiples of Bloch-Zener time T_{BZ}. Second, lots of particles are localized at the center and form a belt. Third, one can observe that the enveloping structure is overlaid by a breathing mode of smaller amplitude. The outside breathing mode is formed by Bloch oscillation and Landau-Zener tunneling for particles in the upper excited Bloch band with period $T_{\mathrm{BZ}} = T_B$. The inside breathing mode is formed by Bloch oscillation for particles remaining in the lower Bloch band with period $T_1 = T_B/2$. The center is the localized belt. In Fig. 4(b) we show the dynamical evolution of the momentum distribution. The strip structure disappears and the windmill structure appears with the center

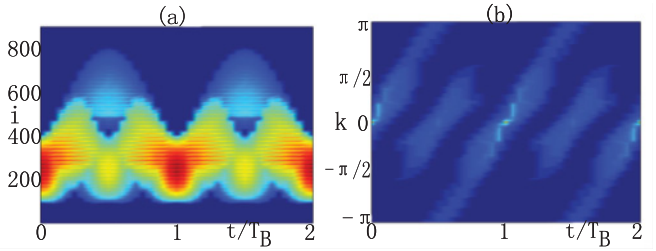

FIG. 5. (Color online) The dynamical evolution of density profile (a) and momentum distribution (b) for the 80-particle system with $F = 0.01$, $\delta = 0.08211$, and $V_H = 4 \times 10^{-5}$.

at $(nT_B, k = 0)$ $(n \in \mathbb{N})$. In this picture we cannot distinguish the two parts of the particles, and lots of particles are localized at an area of $k \approx 0$ all the time. Foremost, the momentum distribution reconstructs at integer multiples of T_{BZ}. The dynamical evolution of the condensate fraction is shown in Fig. 4(c), As the initial state is a localized state, there are many particles with high momentum; right after turning off the trap the condensate fraction decreases quickly, and it reconstructs at $t = T_{\mathrm{BZ}}$. As a lot of particles add in, the initial state becomes a localized state and one can observe breathing mode dynamical evolution of the density profile. In order to observe the oscillating mode and Landau-Zener tunneling, we have to reduce the localization of the initial state by decreasing the strength of the harmonic trap. The dynamics of the system after decreasing the strength of trap is shown in the second column of Fig. 4. For the density distribution we actually see the oscillating mode, but we cannot see the Landau-Zener tunneling clearly. At time range $(T_B/4, 3T_B/4)$, the particles in the upper excited Bloch band and the lower Bloch band are overlapped in real space. This is due to the available interval for the motion being $L \approx 4/F = 80$ for a system with $F = 0.05$, but the size of the system is about $S \approx 300$. It is clear that $S > L$ and the overlapped structure appears. After decreasing the strength of the trap, the strip structure reappears in the dynamical evolution of the momentum distribution instead of the windmill structure. Furthermore, the momentum distribution between the particles in the upper excited and lower Bloch band are distinguishable despite the fact that they are overlapped in real space. For the condensate fraction, the curve is flat again for the time short after turning off the trap.

So in order to observe the oscillating mode of dynamics and Landau-Zener tunneling, one has to let $L > S$. Now we have to decrease the strength of force F to achieve a bigger available interval for the motion. Once F is changed, we have to change δ too to make $E_0 = 0$ for the system still with Bloch-Zener time $T_{\mathrm{BZ}} = T_B$. Furthermore, we have to choose a small δ to achieve the big enough Landau-Zener tunneling probability, otherwise we only see the Bloch oscillation but cannot see the Landau-Zener tunneling. In Fig. 5(a), we show the dynamical evolution of the density profile for the system with $F = 0.01$, $\delta = 0.08211$, and $T_{\mathrm{BZ}} = T_B$. Now we see the clear signals of Bloch oscillation and Landau-Zener tunneling. The dynamical evolution of the momentum distribution and condensate fraction are similar to Figs. 4(e) and 4(f).

IV. CONCLUSION

In summary, we have studied the dynamics of infinitely repulsive Bose gas in tilted or driven bichromatic optical lattices. Using the Bose-Fermi mapping and exact numerical method, we calculate the one-particle density matrices, density profiles, momentum distributions, natural orbitals, and their occupations (condensate fraction). Both the short-time and long-time dynamical evolution of density profile, momentum distribution, and condensate fraction are studied. The reconstruction of the system at integer multiples of Bloch-Zener time is clearly shown. We also give estimations for how to achieve clear Bloch oscillation and Landau-Zener tunneling in given many-particle systems.

ACKNOWLEDGMENTS

This work has been supported by the NSF of China under Grants No. 10821403 and No. 10974234, programs of the Chinese Academy of Science, and the National Program for Basic Research of MOST.

APPENDIX A: THE EQUAL TIME GREEN FUNCTION FOR HARD-CORE BOSONS

The equal time Green function for the hard-core bosons can be written in the form

$$\begin{aligned} G_{ij}(t) &= \langle \Psi_{\mathrm{HCB}}(t) | b_i b_j^\dagger | \Psi_{\mathrm{HCB}}(t) \rangle \\ &= \langle \Psi_F(t) | \prod_{\beta=1}^{i-1} e^{i\pi f_\beta^\dagger f_\beta} f_i f_j^\dagger \prod_{\gamma=1}^{j-1} e^{-i\pi f_\gamma^\dagger f_\gamma} | \Psi_F(t) \rangle \\ &= \langle \Psi^B | \Psi^A \rangle, \end{aligned} \tag{A1}$$

where $|\Psi_{\mathrm{HCB}}(t)\rangle$ is the wave function of hard-core bosons at time t after releasing from the harmonic trap and $|\Psi_F(t)\rangle$ is the corresponding one for noninteracting fermions. In addition, we denote

$$\begin{aligned} |\Psi^A\rangle &= f_j^\dagger \prod_{\gamma=1}^{j-1} e^{-i\pi f_\gamma^\dagger f_\gamma} |\Psi_F(t)\rangle, \\ |\Psi^B\rangle &= f_i^\dagger \prod_{\beta=1}^{i-1} e^{-i\pi f_\beta^\dagger f_\beta} |\Psi_F(t)\rangle. \end{aligned} \tag{A2}$$

The wave function $|\Psi_F(t)\rangle$ can be easily calculated with the initial wave function $|\Psi_F^G\rangle$,

$$|\Psi_F(t)\rangle = e^{-iH_e^F t} |\Psi_F^G\rangle = \prod_{n=1}^{N} \sum_{l=1}^{L} P_{ln}(t) f_l^\dagger |0\rangle, \tag{A3}$$

with

$$P_{ln}(t) = \sum_{k=1}^{N} e^{-i\varepsilon_k t} P'_{lk} \sum_{j=1}^{N} (P'^*_{jk} P_{jn}), \tag{A4}$$

where we have set $\hbar = 1$ in the evolution operator, and $P(t)$ is the matrix of $|\Psi_F(t)\rangle$ in the same way as $|\Psi_F^G\rangle$. In order to get Eq. (A3), one has to insert $\sum_{j=1}^{L} |\phi_j\rangle\langle\phi_j| = 1$ into it, where $|\phi_j\rangle = \sum_{n=1}^{L} P'_{nj} f_n^\dagger |0\rangle$ is the lowest jth eigenfunction of H_e^F.

We can see that $|\Psi_F(t)\rangle$ is still a product of time-dependent single-particle states.

In order to calculate Ψ^A(and Ψ^B) we notice that

$$\prod_{\gamma=1}^{j-1} e^{-i\pi f_\gamma^\dagger f_\gamma} = \prod_{\gamma=1}^{j-1}[1-2f_\gamma^\dagger f_\gamma]. \tag{A5}$$

Then, the action of $\prod_{\gamma=1}^{j-1} e^{-i\pi f_\gamma^\dagger f_\gamma}$ on the state $|\Psi_F(t)\rangle$ [Eq. (A3)] generates only a change of sign on the element $P_{ln}(t)$ for $l<j$, and one has to add a column to $P(t)$ with element $P_{j,N+1}=1$ and all the others equal to zero for the further creation of a particle at site j. Then

$$\begin{aligned} \left|\Psi^A\right\rangle &= \prod_{n=1}^{N+1}\sum_{l=1}^{L} P_{ln}^A f_l^\dagger |0\rangle\,, \\ \left|\Psi^B\right\rangle &= \prod_{n=1}^{N+1}\sum_{l=1}^{L} P_{ln}^B f_l^\dagger |0\rangle\,, \end{aligned} \tag{A6}$$

where P^A and P^B are obtained from $P(t)$ changing the required signs and adding the new column.

The Green function is written as

$$\begin{aligned} G_{ij}(t) &= \langle 0|\prod_{n=1}^{N+1}\sum_{l=1}^{L} P_{ln}^{B*} f_l \prod_{n'=1}^{N+1}\sum_{l'=1}^{L} P_{ln}^{A} f_l'|0\rangle \\ &= \sum_{l_1\cdots 1_{N+1},l_1'\cdots 1_{N+1}'}^{L} P_{l_1 1}^{B*}\cdots P_{l_{N+1}N+1}^{B*} \\ &\quad \times P_{l_1' 1}^{A}\cdots P_{l_{N+1}' N+1}^{A}\langle 0|f_{l_1}\cdots f_{l_{N+1}} f_{l_{N+1}'}^\dagger \cdots f_{l_1'}^\dagger|0\rangle \\ &= \det[(P^B)^\dagger P^A], \end{aligned} \tag{A7}$$

which requires

$$\langle 0|f_{l_1}\cdots f_{l_{N+1}} f_{l_{N+1}'}^\dagger \cdots f_{l_1'}^\dagger|0\rangle = \varepsilon^{\lambda_1\cdots\lambda_{N+1}}\delta_{l_1 l_{\lambda_1}'}\cdots\delta_{l_{N+1}l_{\lambda_{N+1}}'} \tag{A8}$$

with $\varepsilon^{\lambda_1\cdots\lambda_{N+1}}$ the Levi-Civita symbol and $\lambda = 1\cdots N+1$.

APPENDIX B: THE SINGLE-PARTICLE PROPERTIES OF HAMILTONIAN H_e

First of all, for the field-free case with $F=0$, a straightforward calculation yields the dispersion relation

$$E_{\beta k} = (-1)^{\beta+1}\sqrt{\delta^2 + 4\cos^2(k)} \tag{B1}$$

and corresponding wave functions $|\chi_\beta(k)\rangle$ (Bloch bands and Bloch waves) with the miniband index $\beta = 0,1$. For nonzero F, the spectrum of the Hamiltonian consists of two Wannier-Stark ladders with an offset in between. After introducing translation operator

$$T_m = \sum_{n=-\infty}^{\infty} b_{n-m}^\dagger b_n \tag{B2}$$

and an operator G that causes the inversion of the sign of δ in the Hamiltonian,

$$GH_e(\delta) = H_e(-\delta)G, \qquad [T_m, G] = 0, \tag{B3}$$

an eigenvector $|\Psi\rangle$ of H_e with the eigenvalue $E(\delta,F)$ satisfies

$$\begin{aligned} H_e\{T_{2l}|\Psi\rangle\} &= \{E(\delta,F) - 2lF\}\{T_{2l}|\Psi\rangle\}, \\ H_e\{T_{2l+1}|\Psi\rangle\} &= \{E(-\delta,F) - (2l+1)F\}\{T_{2l+1}|\Psi\rangle\}. \end{aligned} \tag{B4}$$

Thus, the eigenenergies of the Hamiltonian

$$\begin{aligned} E_{0,n} &= E(\delta,F) + 2nF, \\ E_{1,n} &= E(-\delta,F) + (2n+1)F, \end{aligned} \tag{B5}$$

consists of two Wannier-Stark ladders with the corresponding eigenstates $|\Psi_{\beta,n}\rangle = T_{-(2n+\beta)}G^\beta|\Psi\rangle$ [22]. A further calculation can prove that $E_0 \equiv E(\delta,F) = -E(-\delta,F)$.

For an initial state expanded on the Wannier-Stark basis,

$$|\Phi\rangle = \sum_n c_{0,n}|\Psi_{0,n}\rangle + \sum_n c_{1,n}|\Psi_{1,n}\rangle, \tag{B6}$$

the dynamics of $|\Phi\rangle$ under the Hamiltonian H_e is given by

$$|\Phi(t)\rangle = \sum_n c_{0,n}e^{-iE_{0,n}t}|\Psi_{0,n}\rangle + \sum_n c_{1,n}e^{-iE_{1,n}t}|\Psi_{1,n}\rangle. \tag{B7}$$

Expanding Wannier-Stark functions on the Bloch basis,

$$|\Psi_{\beta,n}\rangle = \int_{-\frac{\pi}{2}}^{\frac{\pi}{2}} a_{\beta n}(k)|\chi_0(k)\rangle dk + \int_{-\frac{\pi}{2}}^{\frac{\pi}{2}} b_{\beta n}(k)|\chi_1(k)\rangle dk, \tag{B8}$$

and projecting $|\Phi(t)\rangle$ on the Bloch basis, one can get

$$\begin{aligned} \langle\chi_0(k)|\Phi(t)\rangle &= e^{-iE_0 t}[a_{0,0}(k)C_0(k+Ft) \\ &\quad + a_{1,0}(k)e^{-i(F-2E_0)t}C_1(k+Ft)], \\ \langle\chi_1(k)|\Phi(t)\rangle &= e^{-iE_0 t}[b_{0,0}(k)C_0(k+Ft) \\ &\quad + b_{1,0}(k)e^{-i(F-2E_0)t}C_1(k+Ft)], \end{aligned} \tag{B9}$$

where C_β are the Fourier series of $c_{\beta,n}$:

$$C_\beta(k+Ft) = \sum_n c_{\beta,n}e^{-i2n(k+Ft)}, \tag{B10}$$

which are π periodic. To get Eq. (B9) one has to use $T_{-2n}|\chi_\beta(k)\rangle = e^{-i2nk}|\chi_\beta(k)\rangle$ (translation of Bloch waves). From Eq. (B9), one can see that the dynamics of a particle is characterized by two periods: C_β are functions with a period of

$$T_1 = \frac{\pi}{F}, \tag{B11}$$

whereas the exponential function $e^{-i(F-2E_0)t}$ has a period of

$$T_2 = \frac{2\pi}{F-2E_0}. \tag{B12}$$

T_1 is half of the Bloch time $T_B = 2\pi/F$ for the single-band system ($\delta=0$). In general, if T_1 and T_2 are commensurate,

$$\frac{T_1}{T_2} = \frac{2F}{F-2E_0} = \frac{m}{n} \quad \text{with} \quad n,m\in\mathbb{N}, \tag{B13}$$

thus the wave function is reconstructed at integer multiples of Bloch-Zener time ($T_{BZ} = nT_1$).

[1] F. Bloch, Z. Phys. **52**, 555 (1928).
[2] M. Ben Dahan, E. Peik, J. Reichel, Y. Castin, and C. Salomon, Phys. Rev. Lett. **76**, 4508 (1996).
[3] M. Glück, A. R. Kolovsky, and H. J. Korsch, Phys. Rep. **366**, 103 (2002).
[4] J. Feldmann, K. Leo, J. Shah, D. A. B. Miller, J. E. Cunningham, T. Meier, G. vonPlessen, A. Schulze, P. Thomas, and S. Schmitt-Rink, Phys. Rev. B **46**, 7252 (1992).
[5] T. Pertsch, P. Dannberg, W. Elflein, A. Brauer, and F. Lederer, Phys. Rev. Lett. **83**, 4752 (1999).
[6] R. Morandotti, U. Peschel, J. S. Aitchison, H. S. Eisenberg, and Y. Silberberg, Phys. Rev. Lett. **83**, 4756 (1999).
[7] L. D. Landau, Phys. Z. Sowjetunion **2**, 46 (1932).
[8] C. Zener, Proc. R. Soc. London **137**, 696 (1932).
[9] E. Majorana, Nuovo Cimento **9**, 43 (1932).
[10] E. C. G. Stückelberg, Helv. Phys. Acta **5**, 369 (1932).
[11] B. P. Anderson and M. A. Kasevich, Science **282**, 1686 (1998).
[12] B. Rosam, K. Leo, M. Gluck, F. Keck, H. J. Korsch, F. Zimmer, and K. Kohler, Phys. Rev. B **68**, 125301 (2003).
[13] H. Trompeter, T. Pertsch, F. Lederer, D. Michaelis, U. Streppel, A. Brauer, and U. Peschel,Phys. Rev. Lett. **96**, 023901 (2006).
[14] I. Bloch, J. Dalibard, and W. Zwerger, Rev. Mod. Phys. **80**, 885 (2008).
[15] A. Görlitz, T. Kinoshita, T. W. Hänsch, and A. Hemmerich, Phys. Rev. A **64**, 011401(R) (2001).
[16] S. Fölling *et al*., Nature **448**, 1029 (2007).
[17] G. Ritt, C. Geckeler, T. Salger, G. Cennini, and M. Weitz, Phys. Rev. A **74**, 063622 (2006).
[18] T. Salger, C. Geckeler, S. Kling, and M. Weitz, Phys. Rev. Lett. **99**, 190405 (2007).
[19] T. Salger, G. Ritt, C. Geckeler, S. Kling, and M. Weitz, Phys. Rev. A **79**, 011605(R) (2009).
[20] T. Salger, S. Kling, T. Hecking, C. Geckeler, L. Morales-Molina, and M. Weitz, Science **326**, 1241 (2009).
[21] S. Kling, T. Salger, C. Grossert, and M. Weitz, Phys. Rev. Lett. **105**, 215301 (2010).
[22] B. M. Breid, D. Witthaut, and H. J. Korsch, New J. Phys. **8**, 110 (2006).
[23] B. M. Breid, D. Witthaut, and H. J. Korsch, New J. Phys. **9**, 62 (2007).
[24] B. Wu and Q. Niu, Phys. Rev. A **61**, 023402 (2000).
[25] O. Zobay and B. M. Garraway, Phys. Rev. A **61**, 033603 (2000).
[26] J. Liu, L. B. Fu, B.-Y. Ou, S.-G. Chen, D. I. Choi, B. Wu, and Q. Niu, Phys. Rev. A **66**, 023404 (2002).
[27] E. M. Graefe, H. J. Korsch, and D. Witthaut, Phys. Rev. A **73**, 013617 (2006).
[28] D. Witthaut *et al*., e-print arXiv:1012.2896 (2010).
[29] M. Girardeau, J. Math. Phys. **1**, 1268 (1960).
[30] M. Girardeau, E. M. Wright, and J. M. Triscari,Phys. Rev. A **63**, 033601 (2001).
[31] A. Minguzzi *et al*., Phys. Lett. A **294**, 222 (2002).
[32] D. M. Gangardt, J. Phys. A **27**, 9335 (2004).
[33] B. Paredes *et al*., Nature (London) **429**, 277 (2004).
[34] T. Kinoshita *et al*., Science **305**, 1125 (2004).
[35] M. Rigol and A. Muramatsu, Phys. Rev. A **72**, 013604 (2005); **70**, 031603(R) (2004).
[36] M. Rigol and A. Muramatsu, Phys. Rev. Lett. **93**, 230404 (2004); **94**, 240403 (2005).
[37] P. Jordan and E. Wigner, Z. Phys. **47**, 631 (1928).
[38] X. Cai, S. Chen, and Y. Wang, Phys. Rev. A **81**, 023626 (2010); **81**, 053629 (2010).
[39] O. Pensose and L. Onsager, Phys. Rev. **104**, 576 (1956).
[40] T. Hartmann, F. Keck, H. J. Korsch, and S. Mossmann, New J. Phys. **6**, 2 (2004).